ACS APPLIED MATERIALS & INTERFACES

Research Article

www.acsami.org

Surface Disinfection Enabled by a Layer-by-Layer Thin Film of Polyelectrolyte-Stabilized Reduced Graphene Oxide upon Solar Near-Infrared Irradiation

Liwei Hui,[†,‡] Jeffrey T. Auletta,[§] Zhiyu Huang,[†,‡] Xiang Chen,[†,‡] Fei Xia,[†,‡] Shangfeng Yang,[†,‡] Haitao Liu,[§] and Lihua Yang*[,†,‡]

[†]CAS Key Laboratory of Materials for Energy Conversion, and [‡]Department of Materials Science and Engineering, University of Science and Technology of China, Hefei, Anhui 230026, China

[§]Department of Chemistry, University of Pittsburgh, Pittsburgh, Pennsylvania 15260, United States

Supporting Information

ABSTRACT: We report an antibacterial surface that kills airborne bacteria on contact upon minutes of solar near-infrared (NIR) irradiation. This antibacterial surface employs reduced graphene oxide (rGO), a well-known near-infrared photothermal conversion agent, as the photosensitizer and is prepared by assembling oppositely charged polyelectrolyte-stabilized rGO sheets (PEL-rGO) on a quartz substrate with the layer-by-layer (LBL) technique. Upon solar irradiation, the resulting PEL-rGO LBL multilayer efficiently generates rapid localized heating and, within minutes, kills >90% airborne bacteria, including antibiotic-tolerant persisters, on contact, likely by permeabilizing their cellular membranes. The observed activity is retained even when the PEL-rGO LBL multilayer is placed underneath a piece of 3 mm thick pork tissue, indicating that solar light in the near-infrared region plays dominant roles in the observed activity. This work may pave the way toward NIR-light-activated antibacterial surfaces, and our PEL-rGO LBL multilayer may be a novel surface coating material for conveniently disinfecting biomedical implants and common objects touched by people in daily life in the looming postantibiotic era with only minutes of solar exposure.

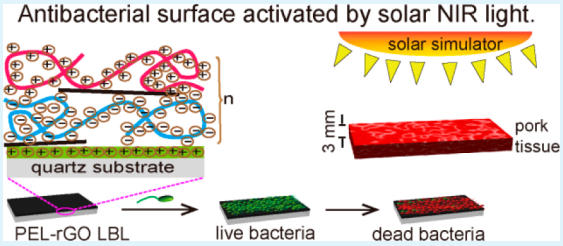

KEYWORDS: *graphene, antibacterial, surface, solar, photothermal*

INTRODUCTION

Human's ever-growing demand for healthy living spurs the ever-lasting development of antibacterial materials. Antibacterial surfaces, in particular, are a high research priority, as bacteria prefer to colonize a solid substrate if available rather than dwell in a planktonic state[1] and, in doing so, may render the substratum surfaces dysfunctional and/or infection-transmissive.[2−4] For example, surfaces of common objects touched by people in daily life (e.g., doorknobs and keyboards), if not intrinsically antibacterial, often transmit infections by airborne bacteria. To be antibacterial, surfaces require modifications.[5,6] Techniques for this purpose include coating the surfaces with certain polymers (e.g., poly(ethylene glycol), poly(4-vinyl-*N*-alkylpyridinium bromide), and zwitterionic polymers) that repel bacterial attachment and/or kill bacteria on contact, modifying the micro- and nanoscale surface topographical features to control bacterial attachment/survival, and impregnating the surfaces with antimicrobial agents (e.g., silver ions) that release into the surrounding solution and kill bacteria therein.[5−10] Recently, photoactivated antibacterial surfaces have attracted intensive investigations. One prominent example is titanium oxide (TiO_2) thin film, which eradicates bacteria via photocatalytic activity upon irradiation of ultraviolet (UV) light; excitation wavelengths are extended to the visible (vis) region for TiO_2 thin films doped with other metals (e.g., silver) and anions (e.g., sulfur) as well as other semiconductor materials (e.g., ZnO).[6,11,12] To activate these photoactivated antibacterial surfaces, an external light source is required. Frequently, it is a single-wavelength laser. Recently, broad-band solar light has been employed as alternative to laser light, for activating antibacterial surfaces including sulfur-doped TiO_2,[13] N-doped TiO_2 thin films,[14] TiO_2−nanoparticle-impreganated polymer matrix,[15] TiO_2 thin film coated with graphene oxide (GO) nanosheets,[16] TiO_2 thin film coated successively with Ag nanoparticles and Ag-TiO_2 nanocomposites,[17] Cu_2O-nanoparticle-sensitized ZnO nanorod arrays on indium−tin−oxide-coated glass substrates,[18] sputtered TiON on polyester surfaces,[19] and textile coated with graphene/TiO_2 composites.[20] Though diverse, these photoactivated antibacterial surfaces usually act via the photocatalytic property of semiconductor materials such as TiO_2 upon irradiation by light in the UV and/or visible regions.

It is known that UV light is carcigenous,[21,22] and light in the UV−vis region has limited tissue penetration depth. Moreover,

Received: March 6, 2015
Accepted: April 23, 2015
Published: April 23, 2015

DOI: 10.1021/acsami.5b02008
ACS Appl. Mater. Interfaces 2015, 7, 10511−10517

the photocatalytic property of TiO_2 may accelerate sunlight's photodamage to human skin.[23] These factors may severely impede the applications of the above photoactivated antibacterial surfaces in biomedical fields especially as coatings for biomedical implants. In addition, only ~5% of solar energy on earth surface is in the UV region, which may limit the efficiency of solar light in activating the above antibacterial surfaces. Having these concerns in mind and noticing that ~55% of solar energy at earth surface is in the near-infrared (NIR) region, we developed a photoactivated antibacterial surface that acts responsively to solar light with NIR irradiation.

As a proof-of-concept, we use reduced graphene oxide (rGO), a well-known NIR photothermal conversion agent[24−28] with a broad absorption spectrum, as the photosensitizer, and prepare rGO-based thin film on a quartz substrate via the layer-by-layer (LBL) technique with oppositely charged polyelectrolyte-rGO complexes (i.e., rGO functionalized with polyelectrolytes (PELs) via noncovalent adsorption on rGO basal plane) (Figure 1). Our results suggest that, upon simulated

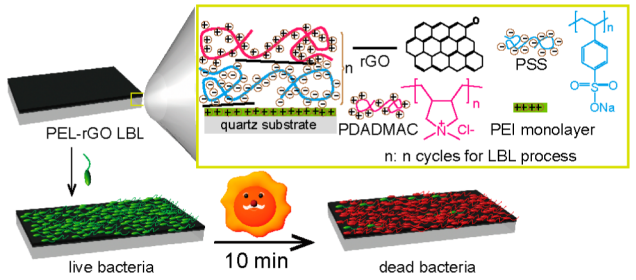

Figure 1. Schematic illustration of a $(PSS\text{-}rGO/PDADMAC\text{-}rGO)_n$ multilayer on a quartz substrate (where n is the number of LBL cycles repeated in multilayer preparation), which is prepared via the LBL technique with the oppositely charged PSS-rGO and PDADMAC-rGO complexes, and kills >90% airborne bacteria on contact upon minutes of solar irradiation.

solar irradiation, the resulting PEL-rGO LBL multilayer generates rapid localized heating and kills >90% airborne bacteria on contact within minutes likely by permeabilizing the bacterial membranes, and solar light in the near-infrared region may play dominating roles in the observed activity. This study suggests that our PEL-rGO LBL multilayer may offer safe and convenient surface disinfection for both biomedical implants and common objects touched by people in daily life in the looming postantibiotic era.

MATERIALS AND METHODS

PEL-rGO Complex Preparation. Graphite oxide (GtO) was prepared following a modified Hummers' method using an extended 5-day oxidation period[29,30] and characterized with thermogravimetric analysis (TGA) and Fourier transform infrared spectroscopy (FT-IR), as described in detail in our prior work.[31]

GO was prepared by sonicating the GtO powder dispersion in Millipore water (5 mg/mL) in a glass vial with a water-bath sonicator at output energy of 200 W for 10 min; the resulting GO dispersion was used within 30 min.

rGO was prepared by reducing GO with hydrazine (85%, Sinopharm Chemical Reagent Co., Ltd.) in the presence of a polyelectrolyte, poly(sodium 4-styrenesulfonate) (PSS) (Mw 70 000, Sigma-Aldrich) or poly(diallyldimethylammonium chloride) (PDADMAC) (Mw 200 000−350 000, 20% in H_2O, Sigma-Aldrich). Specifically, GO dispersion in a flask was mixed with a polyelectrolyte (GO:polyelectrolyte = 1:10, mass ratio) via vortex for over 1 min, followed by addition of hydrazine (hydrazine:GO = 50 μL:5 mg). The resulting mixture was refluxed at 90 °C for 24 h in a water bath, which yielded the PEL-rGO complex dispersion as a black suspension. After having been cooled to room temperature, the resulting PEL-rGO complex suspension was filtered through mixed cellulose ester membrane with pore size of 0.22 μm, to remove excess free polyelectrolyte molecules, followed by washing extensively with Millipore water. The residue on the membrane was redispersed into Millipore water of the expected amount, which yielded the PEL-rGO complex dispersion at approximately 2−3 mg/mL; the concentration was estimated by dividing the innitial GtO mass with the final suspension volume. The same procedure was used for preparing both PSS-rGO and PDADMAC-rGO complexes.

UV−vis−NIR spectra of the dispersions of GO, PSS-rGO, and PDADMAC-rGO in Millipore water were measured with a UV−vis−NIR spectrometer (UV-3600, Shimadzu), with those of the PSS and PDADMAC solutions in Millipore water as controls. Before FT-IR and TGA analysis, dispersions of GO, rGO, PSS, PSS-rGO, PDADMAC, and PDADMAC-rGO were lyophilized for 48 h. FT-IR spectra were collected with an FT-IR spectrometer (TENSOR27, BRUKER) at the wavelength range 400−4000 cm^{-1} at a resolution of 2 cm^{-1}. TGA analysis was performed with a thermogravimetry analyzer (DTG-60H, Shimadzu) by heating the sample under N_2 flow from room temperature to 700 °C at 10 °C/min.

PEL-rGO LBL Thin Film Preparation. Prior to the LBL procedure, a quartz substrate (10 × 25 × 1.2 mm^3) was pretreated with piranha solution (H_2SO_4/H_2O_2 7:3, v/v) for 1 h at 90 °C, rinsed thoroughly with Millipore water, and then dried under gentle N_2 flow. The as-treated substrate was subsequently immersed into polyethylenimine (PEI, Mw 25 000 Sigma-Aldrich) solution (5 mg/mL in Millipore water) for 40 min, to coat the substrate with PEI monolayer that facilitates the subsequent LBL process, and then into Millipore water for 2 min to remove excess PEI molecules. The resulting PEI-monolayer-coated substrate was subsequently immersed successively into a PSS-rGO complex dispersion (0.75 mg/mL in Millipore water) for 30 min, Millipore water for 1 min (to remove excess PSS-rGO complexes), a PDADMAC-rGO complex dispersion (0.75 mg/mL in Millipore water) for 30 min, and Millipore water for 1 min (to remove excess PDADMAC-rGO complexes); this LBL cycle was repeated for n times, leading to $(PSS\text{-}rGO/PDADMAC\text{-}rGO)_n$ LBL multilayer. The as-prepared LBL film was dried under a gentle N_2 stream and stored in a sterile Petri dish before following experiments. The $(PSS/PDADMAC)_n$ LBL thin film was prepared via a similar procedure but with PSS (3.75 mg/mL) and PDADMAC (3.75 mg/mL) solutions.

The UV−vis−NIR absorption spectra of the as-prepared LBL thin films were recorded using a UV−vis spectrometer (UV-3600, Shimadzu). Water contact angles were measured using a contact angle goniometer (CAM 200, KSV) in the water phase. Surface morphology and *in situ* energy dispersive X-ray (EDX) spectra of the as-prepared LBL thin films after gold sputtering (for 120 s) were obtained with a field emission scanning electron microscope (SEM, Sirion200, FEI). Zeta-potentials of PSS-rGO and PDADMAC-rGO complexes were obtained by characterizing the complex dispersion in Millipore water (0.2 mg/mL) after brief sonication (with a water bath soniator at 100 W for 3 min) with a zeta-potential analyzer (Zetasizer Nano ZS90, Malvern) at 25 °C. Each sample was measured three times, each of which was performed for 13 runs. The reported results are averages of three-time results. Atomic force microscopy (AFM) images were obtained by dispersing a PEL-rGO complex (either PSS-rGO or PDADMAC-rGO) into Millipore water (at 0.02 mg/mL), dropping the resulting PEL-rGO complex dispersion (10 μL) onto a freshly cut mica sample, followed by air-drying at room temperature, and then the sample was imaged under an AFM microscope with tapping mode (DI MultiMode V, Veeco); the results were analyzed using Nanoscope Analysis Software.

Photothermal Conversion Characterizations. The kinetics in temperature rise of an LBL thin film during a 10 min light irradiation was monitored by recording its thermographs with an infrared thermal camera (ICI 7320, Infrared Camera Inc.). Simulated solar irradiation was obtained with a solar simulator (Oriel So13A, Newport) (AM 1.5 G) at one sun. Laser irradiation was obtained with an 850 nm laser at

DOI: 10.1021/acsami.5b02008
ACS Appl. Mater. Interfaces 2015, 7, 10511−10517

0.1 W/cm^2, which corrseponds to the irradiance of one sun. Surface temperatures at the center of irradiation zone on an LBL film were extracted from the as-obtained thermographs.

CFU-Counting Antibacterial Assays. Dehydrated Mueller–Hinton (MH) medium formulation and Tryptic Soy Broth (TSB) medium formulation were purchased from Qingdao Hope Bio-Technology (Qingdao, China) and used as supplied to prepare the Mueller–Hinton agar plates and TSB broth, respectively.

To assess the activity of an LBL thin film against wild-type bacteria, assays were carried out using *E. coli* (ATCC 25922) and *P. aureginosa* (ATCC 25873) as representative strains for Gram-negative bacteria, while *S. aureus* (*ATCC 25923*) *and B. subtilis* (*ATCC 6051*) stains are representative Gram-positive bacteria. There were 3–5 individual colonies inoculated into sterile fresh TSB broth (4 mL), followed by incubation at 37 °C for 16–18 h to stationary phase. The bacterial cells were harvested and washed twice with sterile saline (0.9% NaCl) via centrifugation (5810R, Eppendorf) at 710 *g* for 3 min and adjusted with sterile saline in a commercial spraying bottle to achieve a final bacterial number density of ∼5 × 10^8 CFU/mL (colony forming unit per milliliter).

The resulting bacterial suspension was sprayed onto an LBL film on a quartz substrate in a sterile Petri dish 5–7 times, followed by 10 min irradiation with a solar simulator (AM 1.5 G, at one sun); the same solar irradiation was applied when assessing the antibacterial activity of an LBL thin film shielded by a piece of 3 mm thick pork tissue (purchased from a butcher shop). The as-irradiated thin film on a quartz slide was subsequently immersed into sterile fresh TSB broth (6 mL) followed by vortex (LabDancer, IKA) for 1 min; the resulting bacterial suspension was then subjected to 10-fold serial dilutions with sterile saline, and the resulting dilutions (20 μL) were plated onto MH agar plates. This whole procedure should be completed within 30 min. The plated agar plates were subsequently incubated at 37 °C overnight to yield visible colonies. Each assay was performed by plating the as-obtained bacterial suspensions in triplicate, and the reported results are averages of two independent trials (i.e., with two independently prepared LBL films). Controls are those assayed similarly but without solar-light irradiation (i.e., left alone at room temperature for ∼30 min).

The activity of an LBL multilayer surface on a quartz substrate against bacterial persisters was assessed via a similar procedure as described above but with the bacterial persisters prepared using wild-type bacteria, *S. aureus* (ATCC 25923) and *E. coli* (ATCC 25922), according to a previously reported protocol.[32−34] Briefly, for each strain, 3–5 individual colonies were inoculated into sterile fresh TSB broth (4 mL) followed by incubation at 37 °C for 16 h to stationary phase, addition of ampicillin (final concentration of 100 μg/mL), and a 3-h incubation at 37 °C to eliminate nonpersister cells; previous work has demonstrated that this treatment causes lysis of a subset of the bacterial cell population.[32,33] The as-prepared persister cells were harvested via centrifuge (5810R, Eppendorf) at 2627 rcf (relative centrifugal force) for 5 min, washed with sterile saline for 3 times, and then resuspended into sterile saline to ∼5 × 10^8 CFU/mL.

Bacterial Dead/Live Viability Assays. Bacterial live/dead viability assays were performed using a bacterial dead/live viability kit (Molecular Probes), and the staining effects were examined under fluorescence microscopy (IX81, Olympus). *E. coli* (ATCC 25922) and *P. aureginosa* (ATCC 25873) were used as representative strains for Gram-negative bacteria, while *S. aureus* (ATCC 25923) and *B. subtilis* (ATCC 6051) stains were used as representative Gram-positive bacteria. For each bacterial strain, 3–5 individual colonies were inoculated into fresh sterile TSB (4 mL) and then incubated at 37 °C for 16–18 h to the stationary phase. The bacterial cells were harvested and washed with sterile saline via centrifugation at 710 *g* for 3 min, followed by resuspension into sterile saline to ∼10^9 CFU/mL. The resulting bacterial suspension was sprayed on an LBL film on a quartz substrate in a Petri dish with a commercial spray bottle 10 times, followed by simulated solar irrdiation at one sun (corrseponding to 0.1 W/cm^2) for 10 min with a Solar Simulator (Oriel So13A, Newport). Controls are those assayed similarly but without solar-light irradiation (i.e., left alone in the dark at room temperature for ∼30 min).

The as-treated bacteria cells were subsequently stained with SYTO-9 (9.8 μM in Millipore water, 100 μL) and propidium iodide (PI, 58.8 μM in Millipore water, 100 μL), incubated at 37 °C in the dark for 15 min, covered with a coverslip, and imaged under a fluorescence microscopy (IX81, Olympus) with 20× objective lens. FITC and TRITC filters were used for SYTO-9 and PI, respectively. Each sample was imaged at more than five different areas, and the reported results have been checked for consistency with two individual samples.

Statistical Analysis. Statistical comparisons were performed with a student *t* test using the statistical software package BioMedCalc (version 2.9), and *p* values of <0.05 and <0.01 indicate statistical difference and statistically significant difference, respectively.

RESULTS AND DISCUSSION

Preparation of a PEL-rGO LBL thin film on a quartz substrate comprises two steps: preparing the PEL-rGO complex dispersions in Millipore water, and assembling the oppositely charged PEL-rGO complexes on a quartz substrate via the LBL technique (Supporting Information Figure S1).[35] PEL-rGO complexes were prepared by reducing GO with hydrazine in the presence of a polyelectrolyte, poly(sodium 4-styrenesulfonate) (PSS) or poly(diallyldimethylammonium chloride) (PDADMAC). PSS and PDADMAC are oppositely charged and biocompatible,[36] and adsorbates on rGO basal planes via noncovalent adsorptions (Supporting Information Figure S2),[37,38] which not only make the resulting PSS-rGO and PDADMAC-rGO complex dispersions stable without precipitation after standing still for 3 days (Supporting Information Figure S3) but also quench the intrinsic antibacterial activity of rGO[31,39] to enable the expected photoactivated antibacterial activity. UV–vis–NIR absorption spectra (Supporting Information Figure S4a,b), FT-IR absorption spectra (Supporting Information Figure S5), thermogravimetric analysis (Supporting Information Figure S6), and zeta-potential characterizations (Supporting Information Figure S7) consistently confirmed the successful preparation of PSS-rGO and PDADMAC-rGO complexes, which are negatively and positively charged, respectively, and have mass ratios of PEL to rGO estimated to be ∼1:1 (Supporting Information).

We monitor the preparation of a PEL-rGO LBL multilayer by comparing the UV–vis–NIR absorption spectra, the water contact angles, and the scanning electron microscopy (SEM) images before and after the LBL procedure. UV–vis–NIR absorption spectra (Figure 2a and Supporting Information Figure S8) show that a $(PSS\text{-}rGO/PDADMAC\text{-}rGO)_7$ multilayer prepared by repeating the LBL procedure for $n = 7$ times exhibited consistent absorbance of >0.4 across the measured NIR region, indicating that its area-averaged rGO dosage may be high enough for generating bactericidal photothermal effects; further increasing *n* leads to higher NIR absorption but also makes the LBL procedure more time- and effort-consuming. Therefore, we used the $(PSS\text{-}rGO/PDADMAC\text{-}rGO)_7$ multilayer as our PEL-rGO LBL multilayer for all following experiments, with $(PSS/PDADMAC)_7$ multilayer as our PEL LBL multilayer for reference. Water contact angles (Supporting Information Figure S9) reveal that the LBL process rendered the originally hydrophilic piranha-solution-treated quartz substrate (contact angle $\theta = 18°$) significantly more hydrophobic ($\theta \geq 48°$), indicative of formation of LBL thin film over the substrate. SEM images (Figure 2b,c and Supporting Information Figure S10) show that, unlike the PEL multilayer (Supporting Information Figure S10b), the PEL-

DOI: 10.1021/acsami.5b02008
ACS Appl. Mater. Interfaces 2015, 7, 10511–10517

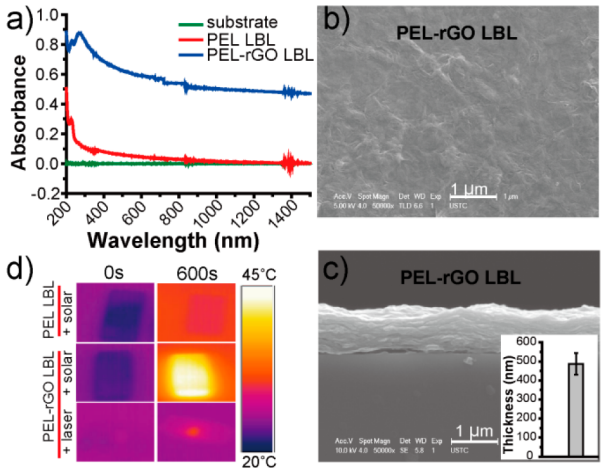

Figure 2. (a) UV−vis−NIR absorption spectra show that a $(PSS\text{-}rGO/PDADMAC\text{-}rGO)_7$ (i.e., PEL-rGO) LBL multilayer consistently exhibited absorbance of >0.4 across the as-measured wavelength-span (200−1500 nm), whereas a $(PSS/PDADMAC)_7$ (i.e., PEL) LBL multilayer did not. The $(PSS\text{-}rGO/PDADMAC\text{-}rGO)_7$ LBL multilayer was used as our PEL-rGO LBL thin film for all following experiments, with the $(PSS/PDADMAC)_7$ LBL multilayer as our PEL LBL thin film for reference. (b, c) SEM images show that the PEL-rGO thin films exhibited a rather rough surface with frequent appearance of wrinkles, with an average film thickness of 487.5 ± 57.5 nm (inset). Data points are reported as mean ± standard deviation (averaged over 3 individual multilayer samples). (d) Thermographs of a PEL-rGO multilayer at 0- and 600-s post-initiation of irradiation with a solar simulator (AM 1.5 G) at one sun. Those of a PEL-rGO multilayer irradiated similarly but with an 850 nm laser at 0.1 W/cm^2 (corresponding to the irradiance of one sun), and those of a PEL multilayer irradiated similarly with a solar simulator were included for reference.

rGO multilayer exhibited a rather rough surface with frequent appearance of wrinkles (Figure 2b), indicative of successful intercalation of rGO. Cross-section-view SEM images of the PEL-rGO multilayer (Figure 2c) further revealed an average multilayer thickness of 487.5 ± 57.5 nm (inset); it should be noted that the film thickness varies significantly even for the same sample (Supporting Information Figure S11). The *in situ* energy dispersive X-ray (EDX) spectra (Supporting Information Figure S10c,d) revealed simultaneous presence of S and Cl elements within an LBL multilayer, confirming successful assembly of PSS and PDADMAC within both PEL-rGO and PEL LBL multilayers. Taken together, these results consistently suggest successful preparation of the expected PEL-rGO LBL multilayer. Moreover, the resulting PEL-rGO LBL multilayer is highly stable even after having been stored at room temperature for 75 days (Supporting Information video).

rGO is well-known for its photothermal effects upon irradiation with an NIR laser.[24−28] To assess whether simulated solar irradiation renders the as-prepared PEL-rGO LBL multilayers efficient in generating rapid localized heating, we recorded the thermographs of a PEL-rGO LBL multilayer during a 10 min period of irradiation with a solar simulator (AM 1.5 G, at one sun) using an infrared thermal camera (Figure 2d and Supporting Information Figure S12a), with the performance of a PEL LBL multilayer as a reference. After 10 min of simulated solar irradiation, the PEL-rGO multilayer generated an average surface-temperature-rise of ∼22 °C (from 20.8 to 42.5 °C) at the center of the irradiation zone (Supporting Information Figure S12b), as compared to <5 °C temperature rise by the PEL multilayer, likely owing to rGO's photothermal effects. In stark contrast, 10 min irradiation with an 850 nm laser at 0.1 W/cm^2, which corresponds to the irradiance of one sun, caused the PEL-rGO multilayer to generate only <4 °C temperature rise in similar assays. Clearly, the broad-band solar irradiation is more efficient in making our PEL-rGO LBL multilayer generate a localized temperature rise than the single-wavelength NIR-laser irradiation of same irradiance, likely owing to rGO's broad absorption.[40]

Rapid localized heating generated by gold nanorod (GNR) conjugated magnetic nanoparticle (MNP) composite (GNR-MNP) upon light irradiation may explain why the composite consistently leads to higher viability loss than does hot-plate heating at the same temperature.[41] Now our PEL-rGO multilayer generates rapid localized surface heating upon 10 min simulated solar irradiation. Is it bactericidal? To address this, we evaluated the activity of our PEL-rGO multilayer against airborne bacteria on contact, as indirect contact is a major pathway for transmission of many diseases.[4] Specifically, we performed colony-forming-unit (CFU) counting antibacterial assays,[10,42] using *E. coli* and *P. aeruginosa* as representative Gram-negative bacteria while *S. aureus* and *B. subtilis* are representative Gram-positive bacteria. Against all four strains tested, the PEL-rGO multilayer killed >90% bacteria within 10 min upon irradiation with a solar simulator (AM 1.5 G) at one sun (Figure 3a), as compared to <20% killing in the dark. In striking contrast, the PEL multilayer barely impaired bacterial survival no matter whether solar irradiation was applied or not, as did the quartz substrates (Figure 3a). Clearly, the PEL-rGO LBL multilayer kills >90% airborne bacteria on contact within minutes upon solar irradiation, likely via rGO's photothermal effects.

Bacterial dead/live viability assays[31,43] under fluorescence microscopy further suggest that, upon solar irradiation, the PEL-rGO LBL thin film may kill bacteria on contact by permeabilizing the bacterial membranes (Figure 3b and Supporting Information Figure S13). SYTO 9 (green) and propidium iodide (PI, red), two nucleic acid stains with distinct spectra characteristics and healthy-membrane-penetrating capabilities, were used to label all and dead bacteria, respectively. For all four bacterial strains tested, cells on a PEL-rGO multilayer stained intensely red upon 10 min solar irradiation, indicative of dead cells with compromised membranes, whereas those assayed similarly but without solar irradiation remained dark in the red channel, indicative of live cells with intact membranes. In contrast, bacteria on a PEL multilayer remained dark in the red channel no matter whether solar irradiation was applied or not, indicative of live cells with intact membranes, similar as those on a quartz substrate. Combined with our CFU-counting antibacterial assays above, these bacterial dead/live viability assays suggest that, upon solar irradiation, the PEL-rGO multilayers may kill bacteria by permeabilizing bacterial membranes (albeit other targets may exist).

Antibacterial materials/molecules that target the barrier function of bacterial membranes are widely viewed as a promising source of novel anti-infective agents especially against antibiotic-resistant bacteria[44,45] and bacterial persisters,[46] which are notorious for their antibiotic tolerance[47] and deteriorating roles in the recurring and chronic infections.[47,48] Eradicating persisters may significantly impact emerging resistance,[34] as persistant presence of persisters effectively acts as a reservoir for resistant mutants.[47,48] Thus, we evaluate the potential of our PEL-rGO multilayer as antibacterial surface in

DOI: 10.1021/acsami.5b02008
ACS Appl. Mater. Interfaces 2015, 7, 10511−10517

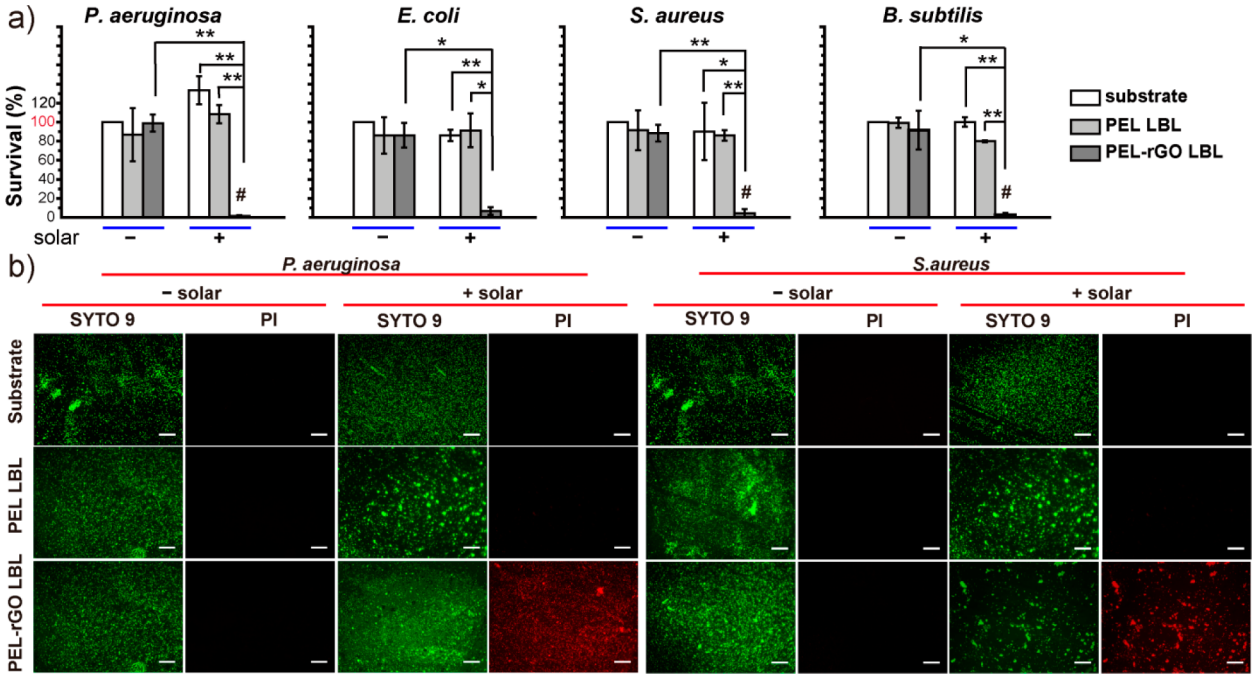

Figure 3. (a) CFU-counting antibacterial assays against four wild-type (wt) bacterial strains consistently reveal that the PEL-rGO LBL thin film, though barely bactericidal when in the dark, killed >90% airborne bacteria on contact within 10 min upon solar irradiation (AM 1.5 G, at one sun). In contrast, the PEL LBL multilayer barely affected bacterial survival no matter whether solar irradiation was applied or not, similar to the behavior of the bare quartz substrate. Data points are reported as mean ± standard deviation. * and ** indicate $p < 0.05$ and $p < 0.01$, respectively. (b) Bacterial dead/live viability assays under fluorescence microscopy show that *P. aeruginosa* and *S. aureus* cells on a PEL-rGO LBL thin film after 10 min irradiation with a solar simulator (AM 1.5 G) stained intensely red, indicative of dead cells with compromised membranes, whereas those treated similarly but without solar irradiation remained dark in the red channel, indicative of live cells with intact membranes. In striking contrast, cells on a PEL LBL thin film or a quartz substrate remained dark in the red channel in similar assays, no matter whether solar irradiation was applied or not. Scale bar = 100 μm.

the looming postantibiotic era by assessing its activity against bacterial persisters. Briefly, CFU-counting antibacterial assays were performed with a similar procedure as described above but against *E. coli* and *S. aureus* persisters prepared with a previously reported protocol.[33,34] Our results (Figure 4) show that the PEL-rGO multilayer, though barely active in the dark, killed >90% *E. coli* and *S. aureus* persisters on contact upon 10 min simulated solar irradiation (AM 1.5 G, at one sun), suggesting the PEL-rGO multilayer as a potential antibacterial surface coating material in the looming postantibiotic era.

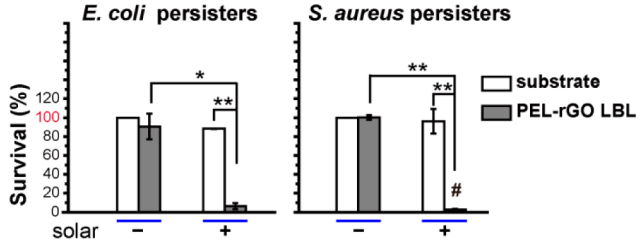

Figure 4. CFU-counting antibacterial assays against bacterial persisters reveal that, upon 10 min solar irradiation (AM 1.5 G, at one sun), PEL-rGO multilayers killed persisters of *E. coli* (left) and *S. aureus* (right) on contact to survival percentages of 6.2% and 2.6%, respectively, as compared to <10% killing when in the dark. In contrast, the bare quartz substrate imposed undetectable effects on bacterial survival no matter whether solar irradiation was applied or not. Data points are reported as mean ± standard deviation. * and ** indicate $p < 0.05$ and $p < 0.01$, respectively.

Simulated solar irradiation offers broad-wavelength light across the UV−vis−NIR window. To assess whether solar light in the NIR region plays dominant roles in the observed activity of our PEL-rGO multilayer, we carried out similar antibacterials assays but with shielding of the LBL-rGO LBL multilayer with a piece of 3 mm thick pork tissue (Figure 5a), a simple but useful setup for simulating an *in vivo* environment[49,50] where NIR light is desired for deep tissue penetration. *P. aeruginosa* and *S. aureus* were used as representative Gram-negative and -positive bacteria, respectively. Our results (Figure 5b,c) reveal that, upon 10 min solar irradiation, the pork-tissue-shielded PEL-rGO LBL multilayer killed *P. aureginosa* and *S. aureus* to survival percentages of 18% and 13%, respectively, indicative of an activity close to that of its tissue-absent counterparts (Figure 3) . Consistently, bacterial dead/live viability assays (Supporting Information Figure S14) reveal that, even in the shade of the pork tissue, bacterial cells on a PEL-rGO multilayer stained intensely red upon 10 min solar irradiation, indicative of dead cells with compromised membranes, as did those on counterparts without shielding by the pork tissue (Figure 3b). Taken together, these results indicate that solar light in the NIR region plays dominant roles in the observed activity of our PEL-rGO LBL multilayer, suggesting its potential as novel surface coating materials for biomedical implants.

CONCLUSION

In summary, we show that a PEL-rGO LBL thin film, which is prepared by assembling the oppositely charged PSS-rGO and PDADMAC-rGO complexes on a quartz substrate with the LBL technique, kills >90% airborne bacteria, including the

DOI: 10.1021/acsami.5b02008
ACS Appl. Mater. Interfaces 2015, 7, 10511−10517

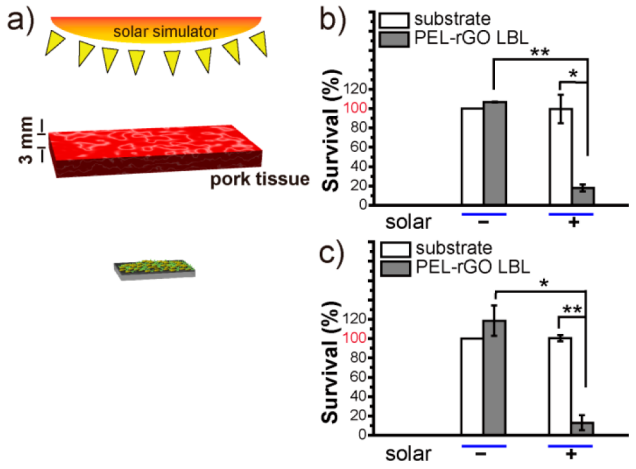

Figure 5. (a) Schematic illustration of a PEL-rGO multilayer that was placed underneath a piece of 3 mm thick pork tissue and, after being sprayed with bacterial suspension, irradiated with a solar simulator (AM 1.5 G). (b, c) CFU-counting antibacterial assays reveal that, upon 10 min solar irradiation, PEL-rGO multilayer shielded by a piece of 3 mm thick pork tissue killed *P.aeruginosa* (b) and *S. aureus* (c) bacteria on contact with survival percentages of 18% and 13%, respectively, as compared to <10% killing when in the dark. Data points are reported as mean ± standard deviation. * and ** indicate $p < 0.05$ and $p < 0.01$, respectively.

antibiotic-tolerant persisters, on contact within 10 min upon simulated solar irradiation at one sun, likely by permeabilizing the bacterial membranes. Solar light in the NIR region may play dominant roles in activating the observed activity of our PEL-rGO LBL multilayer. This work may pave the way toward NIR-light-activated antibacterial surfaces, and the PEL-rGO LBL multilayer may be a novel surface coating material for conferring biomedical implants as well as common objects touched by people in daily life with antiseptic surfaces within minutes of solar exposure.

■ ASSOCIATED CONTENT

Supporting Information

Video of a sample. Figures S1−S14, and additional results and discussion. The Supporting Information is available free of charge on the ACS Publications website at DOI: 10.1021/acsami.5b02008.

■ AUTHOR INFORMATION

Corresponding Author

*E-mail: lhyang@ustc.edu.cn. Phone: +86(551) 6360 6960.

Author Contributions

The manuscript was written through contributions of all authors. All authors have given approval to the final version of the manuscript.

Notes

The authors declare no competing financial interest.

■ ACKNOWLEDGMENTS

We gratefully thank Professors Jun Wang, Guangming Liu, and Zhisheng Ge for use of their facilities. This work was supported in part by the NSFC (11074178 and 21174138) (L.Y.), Ministry of Education of the People's Republic of China (NCET-13-0547 and WK2060200012) (L.Y.), Natural Science Foundation of Anhui Province (1308085QB28) (L.Y.), AFOSR (FA9550-13-1-0083) (H.L.), ONR (N000141310575) (H.L.), and University of Pittsburgh (CRDF fund) (H.L.).

■ REFERENCES

(1) Zobell, C. E. The Effect of Solid Surfaces upon Bacterial Activity. *J. Bacteriol.* **1943**, *46* (1), 39−56.
(2) Arciola, C. R.; Campoccia, D.; Speziale, P.; Montanaro, L.; Costerton, J. W. Biofilm Formation in Staphylococcus Implant Infections. A Review of Molecular Mechanisms and Implications for Biofilm-Resistant Materials. *Biomaterials* **2012**, *33* (26), 5967−5982.
(3) Bazaka, K.; Jacob, M.; Crawford, R.; Ivanova, E. Efficient Surface Modification of Biomaterial to Prevent Biofilm Formation and the Attachment of Microorganisms. *Appl. Microbiol. Biotechnol.* **2012**, *95* (2), 299−311.
(4) Tiller, J. C.; Liao, C.-J.; Lewis, K.; Klibanov, A. M. Designing Surfaces that Kill Bacteria on Contact. *Proc. Natl. Acad. Sci. U.S.A.* **2001**, *98* (11), 5981−5985.
(5) Hasan, J.; Crawford, R. J.; Ivanova, E. P. Antibacterial Surfaces: The Quest for A New Generation of Biomaterials. *Trends Biotechnol.* **2013**, *31* (5), 295−304.
(6) Campoccia, D.; Montanaro, L.; Arciola, C. R. A Review of the Biomaterials Technologies for Infection-Resistant Surfaces. *Biomaterials* **2013**, *34* (34), 8533−8554.
(7) Klibanov, A. M. Permanently Microbicidal Materials Coatings. *J. Mater. Chem.* **2007**, *17* (24), 2479−2482.
(8) Mi, L.; Jiang, S. Integrated Antimicrobial and Nonfouling Zwitterionic Polymers. *Angew. Chem., Int. Ed.* **2014**, *53* (7), 1746−1754.
(9) Zhuk, I.; Jariwala, F.; Attygalle, A. B.; Wu, Y.; Libera, M. R.; Sukhishvili, S. A. Self-Defensive Layer-by-Layer Films with Bacteria-Triggered Antibiotic Release. *ACS Nano* **2014**, *8* (8), 7733−7745.
(10) Ivanova, E. P.; Hasan, J.; Webb, H. K.; Gervinskas, G.; Juodkazis, S.; Truong, V. K.; Wu, A. H. F.; Lamb, R. N.; Baulin, V. A.; Watson, G. S.; Watson, J. A.; Mainwaring, D. E.; Crawford, R. J. Bactericidal Activity of Black Silicon. *Nat. Commun.* **2013**, *4*, Article 2838.
(11) Foster, H.; Ditta, I.; Varghese, S.; Steele, A. Photocatalytic Disinfection Using Titanium Dioxide: Spectrum and Mechanism of Antimicrobial Activity. *Appl. Microbiol. Biotechnol.* **2011**, *90* (6), 1847−1868.
(12) Kikuchi, Y.; Sunada, K.; Iyoda, T.; Hashimoto, K.; Fujishima, A. Photocatalytic Bactericidal Effect of TiO_2 Thin Films: Dynamic View of the Active Oxygen Species Responsible for the Effect. *J. Photochem. Photobiol., A* **1997**, *106* (1), 51−56.
(13) Periyat, P.; Pillai, S. C.; McCormack, D. E.; Colreavy, J.; Hinder, S. J. Improved High-Temperature Stability and Sun-Light-Driven Photocatalytic Activity of Sulfur-Doped Anatase TiO_2. *J. Phys. Chem. C* **2008**, *112* (20), 7644−7652.
(14) Raut, N. C.; Mathews, T.; Ajikumar, P. K.; George, R. P.; Dash, S.; Tyagi, A. K. Sunlight Active Antibacterial Nanostructured N-doped TiO_2 Thin Films Synthesized by an Ultrasonic Spray Pyrolysis Technique. *RSC Adv.* **2012**, *2* (28), 10639−10647.
(15) Kubacka, A.; Serrano, C.; Ferrer, M.; Lünsdorf, H.; Bielecki, P.; Cerrada, M. L.; Fernández-García, M.; Fernández-García, M. High-Performance Dual-Action Polymer−TiO_2 Nanocomposite Films via Melting Processing. *Nano Lett.* **2007**, *7* (8), 2529−2534.
(16) Akhavan, O.; Ghaderi, E. Photocatalytic Reduction of Graphene Oxide Nanosheets on TiO_2 Thin Film for Photoinactivation of Bacteria in Solar Light Irradiation. *J. Phys. Chem. C* **2009**, *113* (47), 20214−20220.
(17) Akhavan, O. Lasting Antibacterial Activities of Ag−TiO_2/Ag/a-TiO_2 Nanocomposite Thin Film Photocatalysts under Solar Light Irradiation. *J. Colloid Interface Sci.* **2009**, *336* (1), 117−124.
(18) Wang, Y.; She, G.; Xu, H.; Liu, Y.; Mu, L.; Shi, W. Cu_2O Nanoparticles Sensitized ZnO Nanorod Arrays: Electrochemical Synthesis and Photocatalytic Properties. *Mater. Lett.* **2012**, *67* (1), 110−112.

(19) Rtimi, S.; Pulgarin, C.; Bensimon, M.; Kiwi, J. Evidence for TiON Sputtered Surfaces Showing Accelerated Antibacterial Activity under Simulated Solar Irradiation. *Sol. Energy* **2013**, *93* (0), 55−62.
(20) Karimi, L.; Yazdanshenas, M.; Khajavi, R.; Rashidi, A.; Mirjalili, M. Using Graphene/TiO_2 Nanocomposite as a New Route for Preparation of Electroconductive, Self-Cleaning, Antibacterial and Antifungal Cotton Fabric without Toxicity. *Cellulose* **2014**, *21* (5), 3813−3827.
(21) Lim, H. W.; Cooper, K. The Health Impact of Solar Radiation and Prevention Strategies: Report of the Environment Council, American Academy of Dermatology. *J. Am. Acad. Dermatol.* **1999**, *41* (1), 81−99.
(22) de Gruijl, F. R. Skin Cancer and Solar UV radiation. *Eur. J. Cancer* **1999**, *35* (14), 2003−9.
(23) Dunford, R.; Salinaro, A.; Cai, L.; Serpone, N.; Horikoshi, S.; Hidaka, H.; Knowland, J. Chemical Oxidation and DNA Damage Catalysed by Inorganic Sunscreen Ingredients. *FEBS Lett.* **1997**, *418* (1−2), 87−90.
(24) Feng, L.; Wu, L.; Qu, X. New Horizons for Diagnostics and Therapeutic Applications of Graphene and Graphene Oxide. *Adv. Mater.* **2013**, *25* (2), 168−186.
(25) Robinson, J. T.; Tabakman, S. M.; Liang, Y. Y.; Wang, H. L.; Casalongue, H. S.; Vinh, D.; Dai, H. J. Ultrasmall Reduced Graphene Oxide with High Near-Infrared Absorbance for Photothermal Therapy. *J. Am. Chem. Soc.* **2011**, *133* (17), 6825−6831.
(26) Feng, L.; Liu, Z. Graphene in Biomedicine: Opportunities and Challenges. *Nanomedicine* **2011**, *6* (2), 317−324.
(27) Li, J.-L.; Tang, B.; Yuan, B.; Sun, L.; Wang, X.-G. A Review of Optical Imaging and Therapy Using Nanosized Graphene and Graphene Oxide. *Biomaterials* **2013**, *34* (37), 9519−9534.
(28) Wu, M.-C.; Deokar, A. R.; Liao, J.-H.; Shih, P.-Y.; Ling, Y.-C. Graphene-Based Photothermal Agent for Rapid and Effective Killing of Bacteria. *ACS Nano* **2013**, *7* (2), 1281−1290.
(29) Hummers, W. S.; Offeman, R. E. Preparation of Graphitic Oxide. *J. Am. Chem. Soc.* **1958**, *80* (6), 1339−1339.
(30) Hirata, M.; Gotou, T.; Horiuchi, S.; Fujiwara, M.; Ohba, M. Thin-film Particles of Graphite Oxide 1:: High-Yield Synthesis and Flexibility of the Particles. *Carbon* **2004**, *42* (14), 2929−2937.
(31) Hui, L.; Piao, J.-G.; Auletta, J.; Hu, K.; Zhu, Y.; Meyer, T.; Liu, H.; Yang, L. Availability of the Basal Planes of Graphene Oxide Determines Whether It Is Antibacterial. *ACS Appl. Mater. Interfaces* **2014**, *6* (15), 13183−13190.
(32) Keren, I.; Kaldalu, N.; Spoering, A.; Wang, Y.; Lewis, K. Persister Cells and Tolerance to Antimicrobials. *FEMS Microbiol. Lett.* **2004**, *230* (1), 13−18.
(33) Allison, K. R.; Brynildsen, M. P.; Collins, J. J. Metabolite-Enabled Eradication of Bacterial Persisters by Aminoglycosides. *Nature* **2011**, *473* (7346), 216−220.
(34) Schmidt, N. W.; Deshayes, S.; Hawker, S.; Blacker, A.; Kasko, A. M.; Wong, G. C. L. Engineering Persister-Specific Antibiotics with Synergistic Antimicrobial Functions. *ACS Nano* **2014**, *8* (9), 8786−8793.
(35) Decher, G. Fuzzy Nanoassemblies: Toward Layered Polymeric Multicomposites. *Science* **1997**, *277* (5330), 1232−1237.
(36) Han, L.; Mao, Z.; Wu, J.; Guo, Y.; Ren, T.; Gao, C. Directional Cell Migration through Cell−Cell Interaction on Polyelectrolyte Multilayers with Swelling Gradients. *Biomaterials* **2013**, *34* (4), 975−984.
(37) Stankovich, S.; Piner, R. D.; Chen, X.; Wu, N.; Nguyen, S. T.; Ruoff, R. S. Stable Aqueous Dispersions of Graphitic Nanoplatelets via the Reduction of Exfoliated Graphite Oxide in the Presence of Poly(sodium 4-styrenesulfonate). *J. Mater. Chem.* **2006**, *16* (2), 155−158.
(38) Wang, S.; Yu, D.; Dai, L.; Chang, D. W.; Baek, J.-B. Polyelectrolyte-Functionalized Graphene as Metal-Free Electrocatalysts for Oxygen Reduction. *ACS Nano* **2011**, *5* (8), 6202−6209.
(39) Tu, Y.; Lv, M.; Xiu, P.; Huynh, T.; Zhang, M.; Castelli, M.; Liu, Z.; Huang, Q.; Fan, C.; Fang, H.; Zhou, R. Destructive Extraction of Phospholipids from Escherichia coli Membranes by Graphene Nanosheets. *Nat. Nanotechnol.* **2013**, *8* (8), 594−601.
(40) Neumann, O.; Urban, A. S.; Day, J.; Lal, S.; Nordlander, P.; Halas, N. J. Solar Vapor Generation Enabled by Nanoparticles. *ACS Nano* **2012**, *7* (1), 42−49.
(41) Ramasamy, M.; Lee, S. S.; Yi, D. K.; Kim, K. Magnetic, Optical Gold Nanorods for Recyclable Photothermal Ablation of Bacteria. *J. Mater. Chem. B* **2014**, *2* (8), 981−988.
(42) Freschauf, L. R.; McLane, J.; Sharma, H.; Khine, M., Shrink-Induced Superhydrophobic and Antibacterial Surfaces in Consumer Plastics. *PLoS One* **2012**, *7* (8), ARTN e40987.
(43) Rapireddy, S.; Nhon, L.; Meehan, R. E.; Franks, J.; Stolz, D. B.; Tran, D.; Selsted, M. E.; Ly, D. H. RTD-1Mimic Containing γPNA Scaffold Exhibits Broad-Spectrum Antibacterial Activities. *J. Am. Chem. Soc.* **2012**, *134* (9), 4041−4044.
(44) Zasloff, M. Antimicrobial Peptides of Multicellular Organisms. *Nature* **2002**, *415*, 389−395.
(45) Hancock, R. E. W.; Sahl, H.-G. Antimicrobial and Host-Defense Peptides as New Anti-infective Therapeutic Strategies. *Nat. Biotechnol.* **2006**, *24* (12), 1551−1557.
(46) Hurdle, J. G.; O'Neill, A. J.; Chopra, I.; Lee, R. E. Targeting Bacterial Membrane Function: An Underexploited Mechanism for Treating Persistent Infections. *Nat. Rev. Microbiol.* **2011**, *9* (1), 62−75.
(47) Lewis, K. Persister Cells, Dormancy and Infectious Disease. *Nat. Rev. Microbiol.* **2007**, *5* (1), 48−56.
(48) Mulcahy, L. R.; Burns, J. L.; Lory, S.; Lewis, K. Emergence of Pseudomonas aeruginosa Strains Producing High Levels of Persister Cells in Patients with Cystic Fibrosis. *J. Bacteriol.* **2010**, *192* (23), 6191−6199.
(49) Li, W.; Wang, J.; Ren, J.; Qu, X. Near-Infrared Upconversion Controls Photocaged Cell Adhesion. *J. Am. Chem. Soc.* **2014**, *136* (6), 2248−2251.
(50) Wang, C.; Tao, H.; Cheng, L.; Liu, Z. Near-Infrared Light Induced in Vivo Photodynamic Therapy of Cancer Based on Upconversion Nanoparticles. *Biomaterials* **2011**, *32* (26), 6145−6154.

DOI: 10.1021/acsami.5b02008
ACS Appl. Mater. Interfaces 2015, 7, 10511−10517